Available online at www.sciencedirect.com
SCIENCE DIRECT®
Diamond and Related Materials 12 (2003) 1793–1799
DIAMOND AND RELATED MATERIALS
www.elsevier.com/locate/diamond

Microstructured diamond X-ray source and refractive lens

Carolina Ribbing[a,*], Björn Cederström[b], Mats Lundqvist[b]

[a]*The Ångström Laboratory, Uppsala University, Box 534, Uppsala SE-751 21, Sweden*
[b]*Royal Institute of Technology, SCFAB, Stockholm SE-106 91, Sweden*

Abstract

This paper treats microstructured CVD diamond in two X-ray applications, a miniature X-ray source and a refractive X-ray lens. The X-ray source consists of boron doped diamond membrane electrodes and an intermediate insulator. The cathode has a pyramidal shape, which is field-emitting and the anode is a metal film on a diamond membrane. Anode radiation emerges through both membrane electrodes. The source has not been vacuum sealed, therefore, all measurements so far have been made in a vacuum chamber. The refractive X-ray lens has saw-tooth geometry and a tunable focal length. It was made by microwave plasma assisted CVD of diamond onto anisotropically etched silicon masters. The lens has been used for one-dimensional focusing of a synchrotron beam to 1.9 μm line width.

Keywords: Micromachining; X-ray; Field emission; CVD

1. Introduction

Diamond is a candidate material for various X-ray applications, such as carrier membrane in X-ray lithography [1] and LIGA [2] masks, as X-ray detector [3], as window on X-ray tubes [4] and detectors [5], as X-ray beam profile monitor [6], as synchrotron X-ray monochromator [7] and as phase plate [8]. Diamond is today more and more often replacing traditional materials in common X-ray components like windows and monochromators. This article describes two new members in the family of diamond-based X-ray associated components: A miniature X-ray source and a refractive X-ray lens.

Diamond's usefulness in X-ray applications is due to a combination of properties. The low atomic number yields a low X-ray attenuation, Fig. 1. All elements with lower atom number suffer from machining difficulties. Together with the high elastic modulus and wet chemistry inertness the low attenuation enables the fabrication of X-ray lithography masks and sub-micron thick diamond windows for X-ray tubes and detectors. Furthermore, diamond is mechanically stable under intense X-ray fluxes and highly resistant to ion erosion, X-ray source construction and field emission applications, desirable properties of a material for lithography. The combination of high thermal conductivity and low thermal expansion yields an excellent thermal shock resistance, important for synchrotron applications.

Most of diamond's properties are due to the exceptionally high bond strength of the covalent C–C bond which anchors every atom to four others. With the advent of the CVD techniques low-cost reproducible diamond growth has become possible on large as well as on microstructured substrates. Furthermore, the diamond can be polished and cut.

Beryllium and silicon are prevalent materials in a variety of X-ray applications. Selected material properties of beryllium and silicon are compared to properties of CVD diamond in Table 1. Beryllium and silicon are not as mechanically and thermally stable as diamond. The low-Z materials beryllium and diamond have a higher ratio of refraction to absorption than silicon. Beryllium has long been a common material for X-ray windows and refractive X-ray lenses. However, it suffers from its toxicity; growth and machining are relatively undeveloped and expensive. On the other hand, for silicon and diamond, microstructure technology supplies superior manufacturing possibilities regarding precision as well as cost. Beryllium has a lower X-ray attenuation than diamond but diamond windows can be made

*Corresponding author. Tel.: +46-18-4717255; fax: +46-18-555095.
E-mail address: carolina.ribbing@angstrom.uu.se (C. Ribbing).

0925-9635/03/$ - see front matter © 2003 Elsevier Science B.V. All rights reserved.
doi:10.1016/S0925-9635(03)00206-1

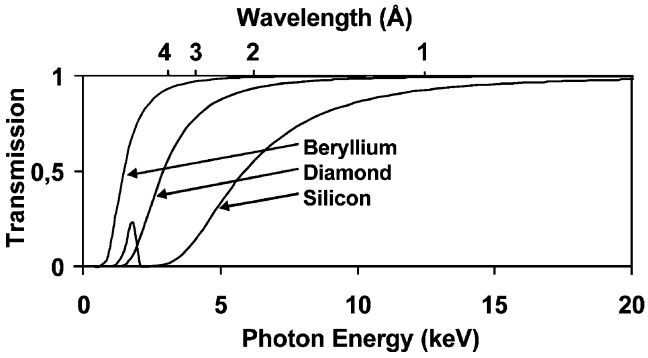

Fig. 1. Transmission of 0–20 keV radiation through 20 μm thick beryllium, diamond and silicon [9].

thinner because of its mechanical properties. Therefore, the performance of diamond windows is comparable to beryllium ones.

Diamond and silicon have the same cubic crystal structure, the diamond structure. One advantage of silicon is its technological maturity, thanks to decades of industrial development within the field of microelectronics. Other simplifying features are relatively low melting point and the presence of a chemically and structurally stable, solid-state oxide. It can be grown in large high-quality single crystals and well-defined processes for patterning, etching and doping exist. Silicon has been tested for X-ray lithography masks and its use in monochromators for synchrotron radiation is commonplace. However, the performance of silicon monochromators varies with the X-ray beam power density, mainly due to thermal deformation of the crystal [7]. Single crystalline diamond is also used as a monochromator material for synchrotron radiation. The relatively weak X-ray absorption of diamond together with its high thermal conductivity and low thermal expansion make the cooling requirements less severe. However, due to the lack of sufficiently large perfect diamond crystals, diamond monocromators are rare.

Some major application areas utilizing X-rays are medicine (treatment and imaging), materials analysis (elemental and structural analysis like X-ray fluorescence, photoelectron spectroscopy and diffraction) and lithography (high resolution, thick resist and LIGA). Within these areas there is a need for microstructured components, e.g. smaller X-ray sources and refractive lenses. Diamond was not our first choice for these applications but was tested because of the properties discussed above. Today, it is one of the most promising materials for our applications.

2. Miniature X-ray source

The initial aim with the X-ray source project was to construct a mm-sized source for irradiation of dilated coronary arteries in vivo. The source was to have a field-emitting cathode to diminish the need of cooling and a high-Z anode to give a high bremsstrahlung yield. The first prototype was made by vacuum brazing grinded tungsten electrodes onto a dense-sintered alumina tube [14]. However, initial cathode tests showed that microstructured diamond cathodes gave more stable field emission currents than microstructured silicon and tungsten cathodes [15]. Since diamond is also a good material for X-ray transmission, work on a chip source with diamond membrane electrodes was initiated [16] (Fig. 2).

The source has a 20 μm thick microstructured diamond membrane with a pyramidal tip as cathode and a 20 μm thick flat membrane with a thin metal film as an anode. Source fabrication and assembling has been described previously [16]. As electrical insulator between electrodes boron nitride, alumina, sapphire and fused quartz have been tested. Acceleration voltages of up to 20 kV have been applied over the electrodes. The diamond-based source is not vacuum encapsulated and consequently all measurements so far have been conducted in a vacuum chamber.

Field-emitting diamond cathodes have been extensively tested in diode and triode set-ups. The most common

Table 1
Selected material properties of CVD diamond in comparison to beryllium and silicon [10–13]

Property	Beryllium	Silicon	CVD diamond
Atomic number	4	14	6
Density (g cm^{-3})	1.85	2.33	3.52
Thermal conductivity (W m^{-1} K^{-1})	230	170	500–2600
Thermal expansion @ 300 K (10^{-6} K^{-1})	11.5	2.5	1.1
Young's modulus (GPa)=Elastic modulus	300	100	1220
Poisson's ratio	0.18	0.28	0.2
Bond strength (kJ/mole) Si–Si, C–C sp^3		220	330–380
Refractive index δ at 10 keV ($\times 10^{-6}$)	3.4	5.0	7.4
Refractive index δ at 20 keV ($\times 10^{-6}$)	0.9	1.2	1.8
Attenuation length at 10 keV (mm)	9.4	0.13	1.3
Attenuation length at 20 keV (mm)	28	1.0	7.7

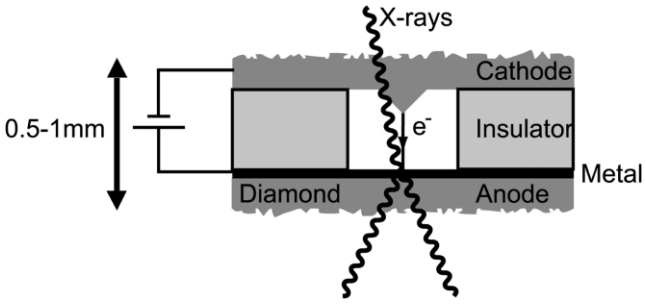

Fig. 2. Design of the diamond membrane based miniature X-ray source (not to scale).

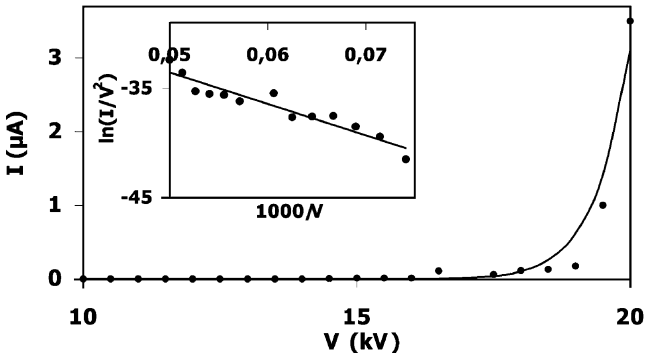

Fig. 3. Current-voltage characteristic of a diamond membrane based X-ray source. The inset shows a Fowler–Nordheim plot.

goal is the construction of flat panel displays, which require a low operating voltage [17]. On the contrary, in the X-ray source a high enough acceleration voltage to produce X-rays in the anode must be applied.

A current–voltage characteristic of a diamond-based source is shown in Fig. 3. The electrode distance of the set-up was 1 mm and the anode metal was silver. The base pressure of the vacuum chamber was 1×10^{-7} torr. Field emission currents generally follow the Fowler–Nordheim relation $I=aV^2e^{-b/V}$ [18]. The solid line in Fig. 3 is a fit of this relation to the measured values. The inset in Fig. 3 shows a linear Fowler–Nordheim plot simply indicating the field emissive origin of the current. The turn-on voltage (giving 1 nA) was 13 kV corresponding to a macroscopic field of 13 V/μm. For construction of the Fowler–Nordheim plot the values below turn-on were disregarded. The turn-on voltage can be tailored by variation of electrode distance or cathode tip radius.

Anode spectra from different diamond-based sources are shown in Fig. 4. The anode metals used were silver, tungsten and gold.

Apart from the coronary application the source may be used in other applications of invasive radiotherapy to replace radioactive isotopes which typically give radiation of unnecessarily high energy. The range in tissue depends on the energy of radiation and the acceleration voltages discussed here are adequate for irradiation of small volumes only. For such short-range irradations, the miniature X-ray source would spare non-target tissue as compared to radioactive sources.

MATLAB simulation of tissue doses administered with the diamond-based source make it possible to decide if it is feasible for therapeutic use [14]. A source encapsulated in 200 μm alumina and 300 μm Teflon was used for dose calculation at 2 and 5 mm distance from the source which is operated at 15 μA and 10, 20 and 30 kV during 100 s, Fig. 5. For the simulation, only the bremsstrahlung part of the radiation emerging through the anode was considered. Variation of the acceleration voltage is possible by adjusting the electrode distance or cathode tip radius. For the coronary application, 10–20 Gy need to be delivered to the artery

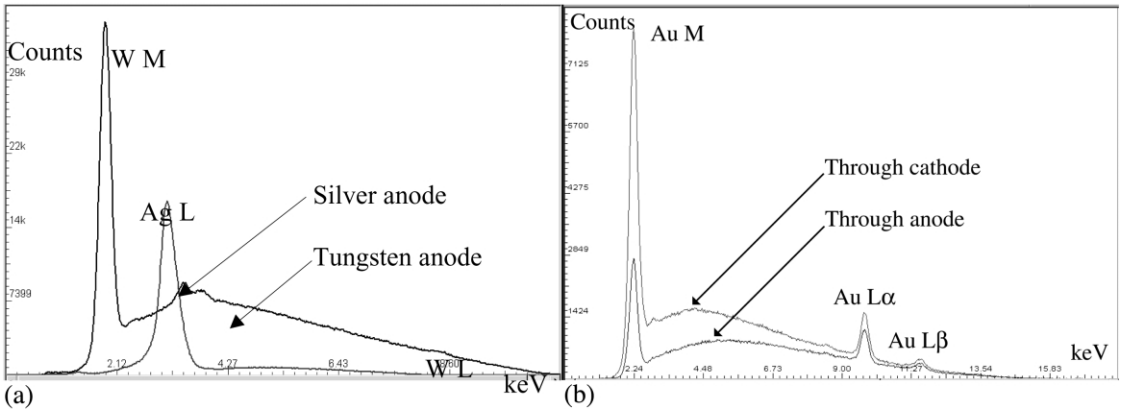

Fig. 4. Spectra collected through the electrodes of miniature X-ray sources: (a) collected through cathodes at an acceleration voltage of 10 kV, tungsten and silver anode, respectively, (b) collected through both electrodes at an acceleration voltage of 15 kV, gold anode. (b) is reprinted from Ref. [16].

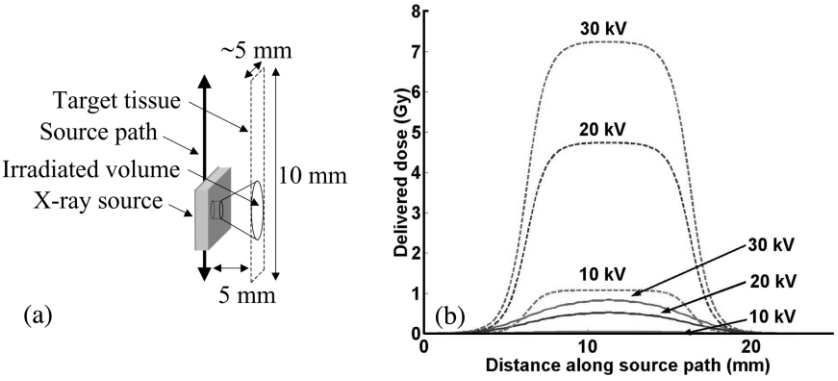

Fig. 5. Simulated tissue doses administered with a miniature X-ray source conducted inside a vessel or lumen (a). The dose was calculated at two distances from the source centre, 2 (dotted line) and 5 mm (solid line), at three different acceleration voltages, 10, 20 and 30 kV. (b). The source is being held still to radiate for 10 s at 10 consecutive stops. The resulting doses are obtained for a total treatment time of 100 s.

wall in less than 20 min. According to the simulations, this dose could be administered with a miniature source operated at 20 kV and 15 μA in approximately 5 min.

For some in vivo applications, management of the generated heat is vital. Temperature simulations indicate that heating of the source operating at 20 kV and 15 μA can be managed [14]. Source geometry and materials could be worked upon such as to dissipate the generated heat in volumes not in contact with tissue. If necessary, the anode could be cooled by flushing physiological saline onto its base. The solution could be injected in a tube inserted along with the electrical cable.

Besides in vivo applications a miniature X-ray source could also serve a purpose in materials analysis. This could be useful for a portable X-ray fluorescence device for field investigations of soil, rock and for satellite born equipment. Initial X-ray fluorescence tests have been made using the diamond-based source for excitation of elemental samples [19].

In vivo insertion of a device powered by tens of kVs is not trivial, but it is really the current that would need to be limited. Therefore, an external current limitation is necessary to prevent injury at ground failure. Safety regulations for cardiac interventions amount to the maximum current allowed (50 μA in the US).

3. Refractive X-ray lens

Because of the weak refraction of X-rays in materials, refractive lenses for X-rays were long considered unfeasible and applicable lenses were not realized until in the late 1990s. A new lens design, the saw-tooth refractive lens, was proposed in 2000 [20] (Fig. 6). Since then it has been fabricated by conventional machining in beryllium as well as microfabricated in silicon and epoxy. When tested in a synchrotron set-up the lenses gave sub-micron focal lines and provided gains of up to 40 [21,22].

In the X-ray range, the complex index of refraction is $n=1-\delta+i\beta$, where δ is the deviation from unity of the refractive part and β is the absorptive part. δ is typically 10^{-6} for 12 keV radiation (1 Å), corresponding to very weak refraction (cf. Table 1). Since $\mathrm{Re}[n]<1$ in the X-ray regime, collecting lenses for X-rays will be concave quite opposite the more familiar case of visible light.

In the lens, rays travelling far away from the center will pass through more surfaces and hence be refracted to a greater extent than more central rays. The tilted saw-tooth structure approximates a planar concave parabolic lens with a radius of curvature, $R=y_g y_t/L \sim \leq 1$ μm, where 2 y_g is the gap between the lens halves, y_t

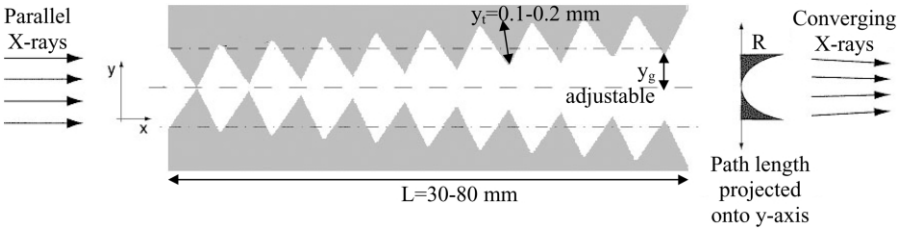

Fig. 6. Geometry of the saw-tooth refractive lens.

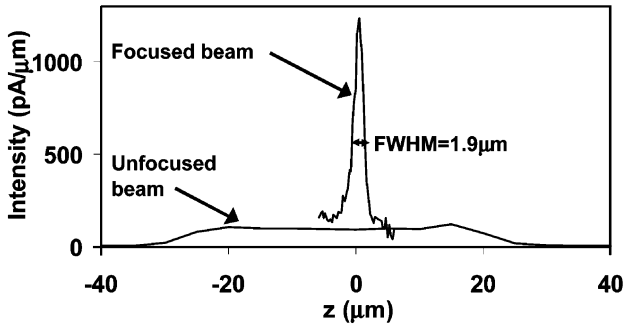

Fig. 7. Derivative of knife-edge scan in the focal plane showing a focal line width of 1.9 μm FWHM at 20 keV. The derivative of a scan of the unfocused beam is included for comparison. $I_{\text{without lens}}$ = 96.6 pA/μm and $I_{\text{with lens}}$ = 1208 pA/μm.

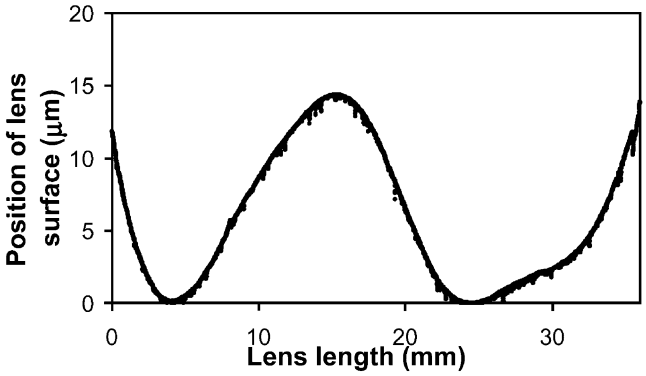

Fig. 8. Surface stylus profiler scan along the lens edge.

is the tooth height and L is the length of the lens. The focal length is $F = R/\delta$ [20]. The saw-tooth lens focuses in one dimension only, i.e. give a focal line. Focusing in two dimensions can be achieved by combining two lenses in series, with the second lens being rotated 90° around the x-axis. Besides the tunable focal length the lens has the advantage of simplified fabrication only involving flat surfaces. It is also more tolerant to surface errors than a single parabolic lens would be, due to the addition of uncorrelated deviations from each surface.

The diamond lenses were fabricated by diamond replication from structured silicon masters. After deposition the silicon was sacrificially removed and the free-standing diamond replicas were glued onto flat glass substrates. The silicon masters were fabricated by standard lithographic patterning and anisotropic wet-etching as described in previous work [22].

The diamond lenses were grown onto the silicon masters by a commercial vendor using microwave plasma assisted CVD from a mixture of hydrogen and hydrocarbon. The resulting diamond lenses had 100 μm high teeth, were 0.4 mm thick and of size 10×40 mm^2.

The lenses were tested in a synchrotron set-up at beamline BM5 at the ESRF in Grenoble. The vertical source size was $d_0 = 80$ μm and the beam was collimated to 60×100 μm^2. The reason for the vertical collimation was that the use of more than the outermost 60 μm part of the teeth gave larger focal line widths. Only half of the lens in Fig. 6 was used in order to avoid alignment problems using two lens halves. The lens was mounted $s_0 = 40$ m from the source. The energy was selected to 20 keV. After alignment the beam profile was measured by scanning a knife-edge in the focal plane at a distance $s_i = 0.62$ m after the lens while measuring the transmitted intensity I with a Si-PIN diode, Fig. 7. The beam intensity $I_{\text{without lens}}$ was measured to 1208 pA/μm. The focal length of the lens was 0.61 m, the focal line width was 1.9 μm FWHM and the gain was $G = I_{\text{with lens}}/I_{\text{without lens}} = 1208/96.6 = 13$.

Theoretically, a focal line width of $d_i = d_0 s_i / s_0 = 80$ μm $\times$ 0.62 m/40 m = 1.24 μm and a gain of 42 would be expected [22]. The discrepancy can be explained by lens bow. The flattest lens had a bow amplitude of 15 μm after mounting, Fig. 8, due to internal stress from the deposition causing twists on silicon removal. Because of the large diamond thickness flat mounting of the lens was difficult.

Scanning electron micrographs of a cross-section of the diamond lenses gave an explanation to the difficulties to use of more than the outermost 60 μm part of the teeth, left micrograph in Fig. 9. Each tooth has a

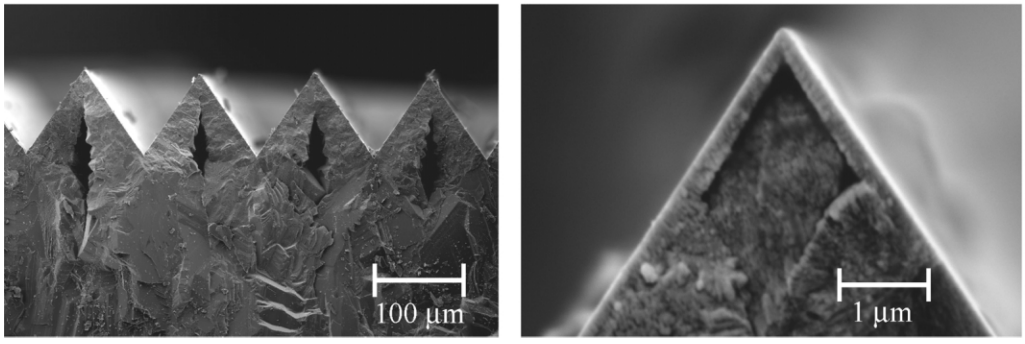

Fig. 9. Scanning electron micrographs showing a cross-section of a diamond lens.

50–100 μm high channel in its lower part, which must evidently impair the focusing properties of the lens. The right micrograph shows the outermost tip of a tooth. Its sharpness reveals satisfying filling of the silicon master. Microspot Raman spectroscopy showed a significant sp^2 content at the outermost microns of tooth tips but otherwise mainly sp^3. The small sp^2 content should be of minor importance for lens performance.

4. Discussion and conclusion

CVD diamond is an interesting material for various X-ray applications. X-rays are used within several fields, for example medicine, materials analysis and lithography. Within these areas there is a need for microstructured components. Two CVD diamond-based structures have been fabricated and tested; a miniature X-ray source and a refractive X-ray lens.

The X-ray source is mm-sized and has been operated at voltages up to 20 kV. It has been used for element identification in an X-ray fluorescence set-up and simulations indicate that therapeutic doses for a cardiovascular application are readily attainable. Vacuum encapsulation of the source remains. In the future, we imagine an all-diamond source with doped electrodes, an undoped insulator and a thin metal layer only as anode.

The refractive X-ray lens has a saw-tooth structure and a tunable focal length. It was originally designed for increasing the photon flux on a scanning slit in a digital imaging system for mammography. However, in the future it may come to serve a similar purpose in an X-ray lithography system. For example as part of an optical system featuring a diminished picture of the flood exposured mask on the substrate resist or by direct writing if the focal spot can be made sufficiently small (in the order of 0.1 μm). It may even be speculated that the use of refractive lenses to increase flux and decrease beam divergence may actually make it possible to replace the synchrotron in X-ray lithography with an X-ray tube for some applications.

The results from the first refractive diamond lenses were not excellent but nevertheless promising. The lenses had a significant bow, which was difficult to decrease on lens mounting because of the large thickness of the lenses. Furthermore, each tooth had an unintentional channel. The origin of the channels may be that the diamond growth was limited by reagent transport rather than by surface kinetics. Another possible explanation is local electric field enhancement at the wedges of the silicon master causing a higher plasma density resulting in increased deposition rate at the tips of the silicon teeth. The bow should be possible to diminish by growth parameter optimisation to reduce stress and by making the lenses thinner to allow for flatter mounting. The channels should be possible to avoid by lowering of the deposition rate or by sample biasing during deposition. Thus, a few simple changes in the deposition process would improve lens performance substantially.

Acknowledgments

The work with the X-ray source was financed by the Swedish Foundation of Strategic Research (SSF) and Summit, a Center of Excellence financed by equal parts from academy, industry and the Swedish Agency for Innovation Systems (VINNOVA).

References

[1] B.-R. Huang, C.-H. Wu, K.-Y. Yang, Mater. Sci. Eng. B75 (2000) 61–67.
[2] M.F. Ravet, F. Rousseaux, Diamond Relat. Mater. 5 (1996) 812–818.
[3] P. Bergonzo, A. Brambilla, D. Tromson, C. Mer, B. Guizard, F. Foulon, et al., Diamond Relat. Mater. 10 (2001) 631–638.
[4] P.K. Bachmann, D.U. Wiechert, in: B. Dischler, C. Wild (eds.), Springer-Verlag, Berlin, Heidelberg, 1998, p. 212–215.
[5] D.A. Fischer, W. Phillips, J. Vac. Sci. Technol. A 10 (4) (Jul/Aug 1992) 2119–2121.
[6] C. Schulze-Briese, B. Ketterer, C. Pradervand, Ch. Brönnimann, C. David, R. Horisberger, et al., Nucl. Instr. Phys. Res. A 467–468 (2001) 230–234.
[7] A.K. Freund, J. Hoszowska, J.P.F. Sellschop, R. Burns, M. Rebak, 11th US National Synchrotron Radiation Instrumentation Conference, AIP Conference Proceedings, 521, 2000, 242–246.
[8] C. Giles, C. Malgrange, J. Goulon, C. Vettier, F. de Bergevin, A. Freund, P. Elleaume, SPIE Vol. 2010 X-Ray and Ultraviolet Polarimetry (1993), p. 136-149.
[9] Data were taken from http://www-cxro.lbl.gov/optical_constants/filter2.html on 020712.
[10] K.E. Spear, J.P. Dismukes (ed.), John Wiley and Sons, Inc., Pennington, New Jersey, 1994.
[11] C. Nordling, J. Österman, Physics Handbook, Studentlitteratur, Lund, Sweden, 1982.
[12] Index data were taken from http://cindy.lbl.gov/optical_constants/getdb2.html on 020712.
[13] Attenuation length data were taken from http://cindy.lbl.gov/optical_constants/atten2.html on 020712.
[14] C. Ribbing, N. Strid, P. Rangsten, J. Tirén, Biomed. Microdevices, 4.4 (2002) 285–292.
[15] P. Rangsten, C. Ribbing, C. Strandman, B. Hök, L. Smith, Sens. Actuators 82 (2000) 24–29.
[16] C. Ribbing, P. Rangsten, K. Hjort, Diamond Relat. Mater. 11 (2002) 1–7.

[17] A. Wisitsora-at, W.P. Kang, J.L. Davidson, D.V. Kerns, S.E. Kerns, J. Vac. Sci. Technol. B 19 (3) (May/June 2001) 971–974.
[18] I. Brodie, P.R. Schwoebel, Proc. IEEE 82 (1994) 1006–1034.
[19] C. Ribbing, K. Hjort, M. Andersson, H. Lundqvist, Rev. Sci. Instrum. 2003, in press.
[20] B. Cederström, R.N. Cahn, M. Danielsson, M. Lundqvist, D.R. Nygren, Nature 404 (2000) 951.
[21] B. Cederström, M. Lundqvist, C. Ribbing, Appl. Phys. Lett. 81 (8) (2002) 1399–1401.
[22] B. Cederström, C. Ribbing, M. Lundqvist, presented at the International Symposium on Optical Science and Technology, SPIE's 47th Annual Meeting, Seattle, WA, USA, 7–11 July 2002.